Published in final edited form as:
IEEE Trans Ultrason Ferroelectr Freq Control. 2012 October ; 59(10): 2201–2209. doi:10.1109/TUFFC.2012.2446.

An Open System for Intravascular Ultrasound Imaging

Weibao Qiu,
Interdisciplinary Division of Biomedical Engineering, The Hong Kong Polytechnic University, Hong Kong SAR, China

Yan Chen,
Department of Applied Physics, The Hong Kong Polytechnic University, Hong Kong SAR, China

Xiang Li,
National Institutes of Health Resource Center for Medical Ultrasonic Transducer Technology and Department of Biomedical Engineering, University of Southern California, Los Angeles, CA

Yanyan Yu,
Interdisciplinary Division of Biomedical Engineering, The Hong Kong Polytechnic University, Hong Kong SAR, China

Wang Fai Cheng,
Department of Applied Physics, The Hong Kong Polytechnic University, Hong Kong SAR, China

Fu Keung Tsang,
Interdisciplinary Division of Biomedical Engineering, The Hong Kong Polytechnic University, Hong Kong SAR, China

Qifa Zhou,
National Institutes of Health Resource Center for Medical Ultrasonic Transducer Technology and Department of Biomedical Engineering, University of Southern California, Los Angeles, CA

K. Kirk Shung,
National Institutes of Health Resource Center for Medical Ultrasonic Transducer Technology and Department of Biomedical Engineering, University of Southern California, Los Angeles, CA

Jiyan Dai, and
Department of Applied Physics, The Hong Kong Polytechnic University, Hong Kong SAR, China

Lei Sun
Interdisciplinary Division of Biomedical Engineering, The Hong Kong Polytechnic University, Hong Kong SAR, China (htsunlei@inet.polyu.edu.hk)

Abstract

Visualization of the blood vessels can provide valuable morphological information for diagnosis and therapy strategies for cardiovascular disease. Intravascular ultrasound (IVUS) is able to delineate internal structures of vessel wall with fine spatial resolution. However, the developed IVUS is insufficient to identify the fibrous cap thickness and tissue composition of atherosclerotic lesions. Novel imaging strategies have been proposed, such as increasing the center frequency of ultrasound or using a modulated excitation technique to improve the accuracy of diagnosis. Dual-mode tomography combining IVUS with optical tomography has also been developed to determine tissue morphology and characteristics. The implementation of these new imaging methods requires an open system that allows users to customize the system for various studies. This paper presents the development of an IVUS system that has open structures to support various imaging strategies. The system design is based on electronic components and printed circuit board, and provides reconfigurable hardware implementation, programmable image processing algorithms, flexible imaging control, and raw RF data acquisition. In addition, the

proposed IVUS system utilized a miniaturized ultrasound transducer constructed using PMN-PT single crystal for better piezoelectric constant and electromechanical coupling coefficient than traditional lead zirconate titanate (PZT) ceramics. Testing results showed that the IVUS system could offer a minimum detectable signal of 25 μV, allowing a 51 dB dynamic range at 47 dB gain, with a frequency range from 20 to 80 MHz. Finally, phantom imaging, *in vitro* IVUS vessel imaging, and multimodality imaging with photoacoustics were conducted to demonstrate the performance of the open system.

I. Introduction

Cardiovascular disease is one of the main causes of morbidity and mortality although there has been increasing utilization of established preventive therapies [1]. Atherosclerosis is a principal consequence of cardiovascular disease; the narrowing of the arteries can lead to ischemia of the heart, resulting in infarction [2]. Clinically, plaque is considered the main determinant of luminal narrowing in atherosclerosis. The risk of atherosclerosis death is increased significantly by the rupture of vulnerable plaque, which may cause thrombus-mediated critical events such as myocardial infarction [3], [4]. There are three main factors to determine plaque vulnerability: thickness of the fibrous cap, size and composition of the atheromatous lipid core, and inflammation within or adjacent to the fibrous cap [5]. The plaque is more prone to rupture with the thin fibrous cap in a high circumferential stress at the luminal border. The risk of plaque rupture also increased if a highly thrombogenic lipid-rich core is included in the plaque with a large size and a low consistent composition [5].

Angiography is a routine diagnostic technique to determine the location and degree of atherosclerotic vessel stenosis [6], but it cannot acquire structural information of the stenotic vessel walls for accurate assessment of atherosclerotic disease burden [7]. Intravascular ultrasound (IVUS) imaging, which can assess the morphological properties of blood vessels directly by cannulating a miniature catheter into the arteries [8]-[10], has been increasingly used for clinical investigations, such as in guiding the placement of stent [11], or evaluation of the therapy strategies and the follow-up examinations in heart transplant recipients [12], [13]. Although IVUS has been extensively used clinically in recent years, IVUS imaging is still insufficient to visualize the thin fibrous cap thickness [14]. The reliability of IVUS is also challenging, especially for characterization of plaque composition [8], [15]. To address these issues, the center frequency of IVUS has been increased for higher resolution [16] and chirp imaging has been used to improve the SNR [17]. Other imaging strategies have been developed recently to investigate atherosclerosis, such as near-infrared spectroscopy [18], [19], optical coherence tomography [10], [20], fluorescence spectroscopy [21], and photoacoustic imaging [22]. These techniques have intrinsic advantages and are sensitive to either plaque structure (luminal diameter, wall thickness, plaque volume, etc.) or composition. However, none of these techniques alone can provide complete information concerning various markers involved in plaque vulnerability and rupture, which may encompass both structure and composition. Integrated probes combining the IVUS technique with these novel imaging modalities could provide valuable information to improve the diagnostic accuracy [23]-[28]. The implementation of these new techniques requires an IVUS system to have open structures, so that it can easily accommodate other techniques to provide comprehensive information. Such an open system should have reconfigurable hardware, programmable processing algorithms, and flexible imaging control to achieve multimodality capability for accurate diagnosis of the cardiovascular diseases.

In this paper, we present the development of such an open IVUS imaging system that can support easy fusion of other techniques for multimodality diagnosis of cardiovascular diseases. This system achieved reconfigurable hardware, programmable processing algorithms, flexible imaging control, and raw RF data acquisition. A field-programmable

gate array (FPGA) was employed as a core microprocessor to accomplish flexibility, diversity, and real-time imaging. Low-noise electronics were used to support large SNR and high-precision data acquisition [29]-[31]. Two high-speed data transfer schemes, the PCI Express (PCIe) interface and USB, were implemented in this system for fast data transmission. The system design was based on electronic components and printed circuit board (PCB) for a compact and cost-effective implementation.

The catheter probe design for IVUS applications is challenging because the size of ultrasonic transducer is extremely small and the center frequency is high. Traditionally, lead zirconate titanate (PZT) is used for IVUS because of its high electromechanical coupling factor and piezoelectric constant. Recently, lead magnesium niobate–lead titanate (PMN–PT) single crystal has demonstrated superior piezoelectric properties for high-frequency, high-performance ultrasonic transducers [32]. PMN–PT single crystal possesses a higher piezoelectric constant and larger electromechanical coupling coefficient than those of conventional PZT ceramics. As a result, it is much more suitable for application in broad bandwidth, high-sensitivity ultrasonic transducers. In this paper, a miniaturized catheter was fabricated using PMN–0.28PT single crystal and demonstrated high sensitivity and broad bandwidth. Moreover, a small rotary motor was developed in this paper to drive the catheter probe to achieve a cross-sectional view of the blood vessels.

This paper is organized as follows: in the Methods section, the open IVUS system development, the miniaturized catheter fabrication, and construction of rotary motor are described in detail. Electronic testing, phantom and tissue imaging results are presented in the Results section, followed by the Conclusions.

II. Methods

The block diagram of the designed open IVUS system is shown in Fig. 1. A miniaturized ultrasonic transducer was placed at distal end of the catheter to transmit and receive ultrasound signals. A customized rotary motor was fabricated to drive the catheter to acquire a cross-sectional view of target vessels. A pulse generator generates high-voltage short pulse to excite the transducer at desired frequency and spectrum specifications. An FPGA-based high-speed digital receiver is developed to process the ultrasound echo signal for programmability and flexibility. The receiver incorporates the front-end electronics such as amplifier, filter, and analog-to-digital converter (ADC), FPGA microprocessor, and the PCIe and USB interfaces. The system is designed on electronic components and PCB for a compact implementation. A personal computer is used for image display and data storage for further investigations. The high-speed data transfer scheme can be chosen between PCIe and USB according to the specific applications.

A. Miniaturized Catheter Probe

A 32-MHz single-element side-view ultrasound transducer was fabricated using PMN–0.28PT single crystal. The transducer was designed using the Piezo CAD simulation software (Version 3.03 for Windows, Sonic Concepts, Woodinville, WA) based on one-dimensional Krimholtz–Leedom–Matthae (KLM) model. The transducer included four components: backing material, active element, matching layer, and metal housing. Parylene C (Specialty Coating Systems, Indianapolis Inc., IN) is used as the matching layer and protecting layer to compensate for the acoustic impedance mismatch between the PMN–0.28PT single crystal and human tissues; it was evaporated onto the transducers by a parylene deposition system (model PDS 2010, Specialty Coating Systems Inc., Indianapolis, IN). A conductive epoxy (E-solder 3022, Von Roll Isola, New Haven, CT) was cast on the single crystal as the backing material of the transducer to enhance the sensitivity. The transducer probe was wired with a flexible metal drive cable (Asahi Intecc Co. Ltd.,

Pathumthani, Thailand). The metal drive cable for the catheter is 1.5 m long and 0.7 mm in diameter.

B. Pulse Generator

The pulse generator designed for this open IVUS system incorporated a bipolar pulse generation scheme. A programmable FPGA component (Cyclone III, EP3C16F-484C6N, Altera Corporation, San Jose, CA) was used to control the timing and spectrum characteristics of the high-voltage short pulse. Therefore, the pulse generator can be easily adjusted to support transducers with different center frequencies, and to match with the spectrum of an individual transducer to acquire the optimized performance. Two MOSFET drivers (EL7158, Intersil Corp., Milpitas, CA) were used to accomplish the voltage level shift and high current output to excite the high-speed MOSFET pair (TC6320, Supertex Inc., Sunnyvale, CA). The MOSFET pair could offer more than 150 Vpp breakdown voltages and a 2 A output peak current, which made it suitable to produce a high-voltage pulse for IVUS imaging. Finally, the pulse generator performance was evaluated by a digital oscilloscope (Wavepro 715Zi, LeCroy Corp., Chestnut Ridge, NY) with a series of attenuators (Mini-Circuits, Brooklyn, NY).

C. Digital Receiver

A low-noise preamplifier (SMA231, Tyco Electronics Co., Berwyn, PA) was used as the first stage to achieve a good SNR, followed by a second-stage amplifier (THS4509, Texas Instruments Inc., Dallas, TX) to achieve adequate amplification gain. A high-speed, 11-bit ADC (ADS5517, Texas Instruments Inc., Dallas, TX) with a maximum sampling rate of 200 megasamples per second (MSPS) was utilized for signal digitization. After digitization, the signal was transferred to the FPGA through a low-voltage differential signaling (LVDS) bus. A high-performance FPGA (Stratix II EP2S60F672C5, Altera Corporation) was employed for programmable signal/image processing and high-speed data transfer. It could achieve various programmable algorithms such as band-pass filter (BPF), Hilbert transform, envelope detection, and digital scan conversion. A 128-Mbit synchronous dynamic random access memory (SDRAM; MT48LC8M16A2, Micron Technology Inc., Boise, ID) was configured for temporary data storage for the FPGA. Finally, the processed images or raw RF data were transferred to a computer through a PCIe interface component (PEX8311, PLX Technology Inc., Sunnyvale, CA) or USB interface component (CY68013A, Cypress, San Jose, CA) for display, storage, or postprocessing.

The performance of the open IVUS system electronics was tested with the following aspects. The linearity and flatness of gain in receiver were tested by a 240-MHz function generator (AFG 3251, Tektronix Inc., Beaverton, OR), and a digital oscilloscope (Wavepro 715Zi, LeCroy Corp.). The noise level of the system was tested by measuring the minimum detectable signal level and dynamic range. A five-cycle sinusoidal signal generated by the function generator was attenuated by a series of attenuators and then sent to the IVUS receiver. After passing through the front-end electronics, the amplitude of the weak signal that could just be identified from the background noise determined the minimum detectable signal level. Given the input range of the high-speed ADC (2 Vpp), the dynamic range can be derived from the gain and the minimum detectable signal level.

As a field-programmable microprocessor, the FPGA can achieve various functionalities traditionally realized by hardware circuitry. Moreover, the functions can easily be changed or modified by reprogramming the FPGA without changing the hardware. Thus, the FPGA technology can significantly improve the system flexibility and diversity by programmable and reconfigurable algorithms. Fig. 2 shows a representative structure of image processing algorithms for real-time IVUS imaging. The entire processing algorithms could be easily

reprogrammed according to different applications. A double data rate LVDS buffer is used to decode the digitized ultrasound echo data through high-speed ADC. Both the rising and falling edges of the clock are employed for data transfer to achieve high data throughput. A BPF based on finite impulse response (FIR) structure is used to remove noise from the spectrum of interest. The coefficient of the BPF is reconfigurable for individual transducers with different center frequency and bandwidth. The filtered signal is then sent to the envelope detector to achieve envelope extraction by the Hilbert transform algorithm. The acquired envelope data then undergo digital scan conversion and logarithmic compression for coordinate conversion and data compression, respectively. A flexible scan converter based on linear interpolation is employed for fast and accurate processing. Finally, image data are sent to a personal computer through the PCIe or USB interface for display and storage. An SDRAM controller is employed to buffer data with external SDRAM for flexible digital scan conversion and logarithmic compression.

D. Rotary Motor

A rotational motor is designed and implemented to acquire cross-sectional views of blood vessels by rotating the catheter. The detailed structure of the rotary motor is shown in Fig. 3. The design used a direct current motor, which was installed in a metal box, to rotate a horizontal bevel gear. The torque transferred from the horizontal bevel gear was passed to a vertical bevel gear fixed on a hollow shaft. The hollow shaft could be rotated at certain speed, driven by the gears and motor. A coaxial cable inside the hollow shaft was connected to an SMA connector to wire the catheter. The other end of the cable was connected to a slip ring (Sen Ring Electronics Co. Ltd., Shenzhen, China). The slip ring is a rotary coupling device which is used to transfer ultrasound signal from the stationary IVUS circuitry to a rotatable catheter. An optical sensor was used to generate a trigger signal for system synchronization.

E. Graphical User Interface Software

The graphical user interface (GUI) software is programmed in Visual C++ and compiled in Visual Studio 2005 Professional Edition (Microsoft Corporation, Redmond, WA) to control, process, and display the real-time images. The GUI software allows the user to operate the system with great ease and flexibility. It controls the center frequency and the number of cycles of the excitation pulse, the BPF parameters to match to individual transducer characteristics, the number of scanlines in each image, and the point length of the scanline. It can also select sole IVUS mode or multimodality mode. In addition to the images, the raw RF data can be saved by the flexible GUI software.

III. Results

The photographs of the open IVUS system prototypes are shown in Fig. 4. Fig. 4(a) shows the entire system. The ultrasound transducer catheter and rotary motor are shown in Fig. 4(b) and Fig. 4(c), respectively. The pulse generator and digital receiver are shown in Fig. 4(d) and Fig. 4(e), respectively, based on an eight-layer PCB design incorporating state-of-the-art electronics.

A. Catheter

The active element of the transducer in the catheter is a piece of 70-μm-thick PMN–0.28PT single crystal with a size of about 0.6 × 0.6 mm. Fig. 5 shows the modeled and the measured pulse–echo waveform and frequency spectrum. The modeled result agreed well with the measured result. The measurement was acquired by a Panametrics 5900PR pulser/receiver (Olympus NDT Inc., Waltham, MA) and a digital oscilloscope (Infinium 54810A, Hewlett-Packard/Agilent Technologies). The receiver gain of 5900PR pulser/receiver is 16 dB. The

measured center frequency of the catheter is about 32 MHz. The −6-dB bandwidth and the insertion loss are 62.7% and 25 dB, respectively.

B. Electronics

Table I summarizes the performance of the IVUS system electronics. The highest amplitude of bipolar pulse was 160 Vpp with adjustable center frequency and bandwidth. Table I also demonstrates that the maximum gain of the front-end electronics is 47 dB with good linearity at a maximum fluctuation of less than ±1.2 dB between 10 and 90 MHz. The minimal detectable signal level of the system receiver is less than 25 μV. Given the input range of the high-speed ADC (2 Vpp), the system can allow a 51 dB dynamic range at 35 MHz center frequency.

C. FPGA Algorithms and Processing Speed

The software-based BPF was programmed in the FPGA to further remove the noise and improve the signal SNR. Quantitative analysis showed that approximately 4.8 dB SNR improvement was achieved after applying the BPF, which increased the system dynamic range to 55.8 dB.

Table II lists FPGA resource utilization in the FPGA for IVUS imaging only. There is a significant amount of resources left to support the combination of other techniques with IVUS for comprehensive analysis of cardiovascular disease.

The algorithmic scheme implemented in the FPGA can achieve high-speed imaging by pipe-line signal processing. The data transfer speed was higher than 150 and 20 MB/s for PCIe or USB interface, respectively. At the image size of 512 × 512 pixels, the frame rate can be higher than 200 and 20 images per second for PCIe and USB, respectively. The current frame rate is limited by the rotary motor and it can be significantly improved if a faster rotary motor is used. With the current utilization of FPGA resources, much more complicated signal processing may be implemented to acquire more useful information than vessel morphology, e.g., virtual histology (tissue characterization based on ultrasound raw RF data).

D. Imaging Experiments

The image quality of the IVUS system was evaluated first by a customized tungsten wire phantom. The wire phantom consisted of four 20-μm-diameter tungsten wires (California Fine Wire Co., Grover Beach, CA) located at different depths. The ultrasound image of this wire phantom is shown in Fig. 6(a) with a dynamic range of 48 dB without noticeable noise.

A tissue-mimicking phantom was fabricated and imaged as shown in Fig. 6(b). The phantom fabrication procedure followed Madsen's method [33]. In short, it consisted of a mixture of deionized water, high-grade agarose, preservative, propylene glycol, filtered bovine milk, and glass beads. The phantom could generate tissue-mimicking attenuation and backscattering in the high-frequency range. The experiment shows that the penetration depth of this IVUS system is more than 4 mm, which is adequate for most IVUS applications.

An *in vitro* coronary artery specimen was used for system evaluation. The designed catheter was inserted into the specimen for cross-sectional imaging. The ultrasound image of the *in vitro* normal swine coronary artery fixed in a water tank is shown in Fig. 7(a). Different layers of the artery can be clearly identified in the ultrasound image. The specimen then underwent a histological process using hematoxylin and eosin (H&E) stain to confirm the IVUS measurement. The histological image captured by microscope (Eclipse TS100 with digital camera DXM 1200C, Nikon Instrucments Inc., Tokyo, Japan) is shown in Fig. 7(b),

demonstrating detailed identification of different layers including intima, media, and adventitia. The geometric dimension and morphology of vessel correlated well between the IVUS image and histological measurement which confirms the accuracy of the open IVUS system.

The result from a multimodality imaging combining IVUS and photoacoustics is shown in Fig. 8. The specimen was from a post-mortem human coronary artery. The experimental setup was similar to Sethuraman's method [22]. An actively Q-switched pulsed laser (Explorer 532 Laser System, Spectra-Physics, Santa Clara, CA) operating at 532 nm wavelength generated very short laser pulses with 240 μJ energy, and the laser light excited the sample from outside. Ultrasound imaging was launched after the acquisition of the photoacoustic signal. The acquired IVUS and photoacoustic images are shown in Fig. 8(a) and Fig. 8(b), respectively. The intensity of the IVUS echo slightly increases in the bottom right corner of the tissue. This difference can be clearly visualized in photoacoustic image, which may indicate a change of tissue composition. The combined image is shown in Fig. 8(c) to show the complementary nature of IVUS and photoacoustic imaging that could be useful for the diagnosis of intravascular diseases. These *in vitro* experiment results clearly demonstrate the capability of multimodality imaging in this open system.

IV. Discussion

The proposed open system is highly programmable for IVUS-related investigations. The open strategy and programmable capability make it suitable for a variety of applications. The imaging characteristics, such as frequency spectrum of the transmitted pulse, parameters of the receiver filter, sampling rate, number of scanlines, and length of scanlines can be configured easily. The raw RF data can also be saved by the system.

The proposed system supports open IVUS imaging with programmable algorithms and easy implementation of novel algorithm verification and multimodality imaging. The image processing algorithms shown in Fig. 2 are the novel approaches achieved in a single FPGA for IVUS imaging. It can be easily replaced with state-of-the-art algorithms. There are still many resources left for IVUS imaging in the FPGA. Novel image processing algorithms such as tissue characterization based on ultrasound raw RF data and penetration improvement based on modulated excitation can be implemented in this open system. Multimodality imaging combining IVUS and photoacoustics demonstrated the flexible capability of the open system. The program in the FPGA of the system was updated accordingly to fulfill the function. The result showed that combining these two imaging modalities could be easily implemented in this open architecture. The system design is based on electronic components and PCB for a highly compact implementation, which facilitates the ultimate integration of a multimodality imaging system. However, some auxiliary parts may have to be added to the open system in practical applications. An external laser was used for light excitation for the current implementation. In the future, a hybrid transducer combining an ultrasound transducer and optical delivery device will be developed for clinical applications.

V. Conclusions

An open system for IVUS imaging was developed and evaluated in this paper. It provides reconfigurable hardware, programmable processing algorithms, flexible imaging control, and raw RF data acquisition for various IVUS applications. We demonstrated that the open structure may enable IVUS to combine with other techniques to facilitate multimodality imaging and comprehensive diagnosis of cardiovascular diseases. In addition, a miniaturized ultrasound catheter probe was designed and fabricated with PMN–PT single crystal to achieve high sensitivity and broad bandwidth. Such an open system can be a valuable

platform to combine different imaging modalities to improve diagnosis accuracy and treatment effectiveness for cardiovascular disease.

Acknowledgments

The authors thank L. P. C. Kwan for help with histology.

The authors thank the Hong Kong Research Grant Council (RGC) General Research Fund (GRF) (PolyU 5301/09E), the Hong Kong Innovative Technology Council (project number ITS/044/09 FP), and the Centre for Smart Materials of the Hong Kong Polytechnic University for financial support.

References

1. Libby P. The forgotten majority: Unfinished business in cardiovascular risk reduction. J Am Coll Cardiol. 2005; 46(7):1225–1228. [PubMed: 16198835]
2. Ross R. Atherosclerosis—An inflammatory disease. N Engl J Med. 1999; 340(2):115–126. [PubMed: 9887164]
3. Virmani R, Kolodgie FD, Burke AP, Farb A, Schwartz SM. Lessons from sudden coronary death: A comprehensive morphological classification scheme for atherosclerotic lesions. Arterioscler Thromb Vasc Biol. 2000; 20(5):1262–1275. [PubMed: 10807742]
4. Pasterkamp G, Falk E. Atherosclerotic plaque rupture: An overview. J Clin Basic Cardiol. 2000; 3(2):81–86.
5. Pasterkamp G, Falk E, Woutman H, Borst C. Techniques characterizing the coronary atherosclerotic plaque: Influence on clinical decision making. J Am Coll Cardiol. 2000; 36(1):13–21. [PubMed: 10898406]
6. Blankenhorn DH, Azen SP, Kramsch M, Mack WJ, Cashin-Hemphill L, Hodis HN, DeBoer LW, Mahrer PR, Masteller MJ, Vailas LI, Alaupovic P, Hirsch LJ. Coronary angiographic changes with lovastatin therapy: The monitored atherosclerosis regression study (MARS). Ann Intern Med. 1993; 119(10):969–976. [PubMed: 8214993]
7. Kastelein JJ, de Groot E. Ultrasound imaging techniques for the evaluation of cardiovascular therapies. Eur Heart J. 2008; 29(7):849–858. [PubMed: 18334471]
8. Nicholls SJ, Sipahi I, Schoenhagen P, Crowe T, Tuzcu EM, Nissen SE. Application of intravascular ultrasound in anti-atherosclerotic drug development. Nat Rev Drug Discov. 2006; 5(6):485–492. [PubMed: 16699493]
9. de Korte CL, van der Steen AFW, Cespedes EI, Paster-kamp G, Carlier SG, Mastik F, Schoneveld AH, Serruys PW, Bom N. Characterization of plaque components and vulnerability with intravascular ultrasound elastography. Phys Med Biol. 2000; 45(6):1465–1475. [PubMed: 10870704]
10. Hartmann M, Huisman J, Bose D, Jensen LO, Schoenhagen P, Mintz GS, Erbel R, von Birgelen C. Serial intravascular ultrasound assessment of changes in coronary atherosclerotic plaque dimensions and composition: An update. Eur J Echocardiogr. 2011; 12(4):313–321. [PubMed: 21421584]
11. Lemos PA, Saia F, Ligthart JMR, Arampatzis CA, Sianos G, Tanabe K, Hoye A, Degertekin M, Daemen J, McFadden E, Hofma S, Smits PC, de Feyter P, van der Giessen WJ, van Domburg RT, Serruys PW. Coronary restenosis after sirolimus-eluting stent implantation: Morphological description and mechanistic analysis from a consecutive series of cases. Circulation. 2003; 108(3): 257–260. [PubMed: 12860901]
12. Kobashigawa JA, Tobis JM, Mentzer RM, Valantine HA, Bourge RC, Mehra MR, Smart FW, Miller LW, Tanaka K, Li H, Gjertson DW, Gordon RD. Mycophenolate mofetil reduces intimal thickness by intravascular ultrasound after heart transplant: Reanalysis of the multicenter trial. Am J Transplant. 2006; 6(5, pt. 1):993–997. [PubMed: 16611335]
13. Kobashigawa JA, Tobis JM, Starling RC, Tuzcu EM, Smith AL, Valantine HA, Yeung AC, Mehra MR, Anzai H, Oeser BT, Abeywickrama KH, Murphy J, Cretin N. Multi-center intravascular ultrasound validation study among heart transplant recipients: Outcomes after five years. J Am Coll Cardiol. 2005; 45(9):1532–1537. [PubMed: 15862430]

14. Mintz GS, Maehara A. Serial intravascular ultrasound assessment of atherosclerosis progression and regression: State-of-the-art and limitations. Circ J. 2009; 73(9):1557–1560. [PubMed: 19638706]
15. Alfonso F, Hernando L. Intravascular ultrasound tissue characterization. I like the rainbow but… what's behind the colours? Eur Heart J. 2008; 29(14):1701–1703. [PubMed: 18559328]
16. Li X, Wu W, Chung Y, Zhou Q, Shung KK. 80-MHz intra-vascular ultrasound transducer using PMN-PT free-standing film. IEEE Trans Ultrason Ferroelectr Freq Control. 2011; 58(11):2281–2288. [PubMed: 22083761]
17. Maresca D, Jansen K, Renaud G, van Soest G, Li X, Zhou Q, de Jong N, Shung KK, van der Steen AFW. Intravascular ultrasound chirp imaging. Appl Phys Lett. 2012; 100(4) art. no. 043703.
18. Waxman S, Dixon SR, L'Allier P, Moses JW, Petersen JL, Cutlip D, Tardif JC, Nesto RW, Muller JE, Hendricks MJ, Sum ST, Gardner CM, Goldstein JA, Stone GW, Krucoff MW. In vivo validation of a catheter-based near-infrared spectroscopy system for detection of lipid core coronary plaques: Initial results of the SPECTACL study. JACC Cardiovasc Imaging. 2009; 2(7): 858–868. [PubMed: 19608137]
19. Schultz CJ, Serruys PW, van der Ent M, Ligthart J, Mastik F, Garg S, Muller JE, Wilder MA, van de Steen AF, Regar E. First-in-man clinical use of combined near-infrared spectroscopy and intravascular ultrasound: A potential key to predict distal embolization and no reflow? J Am Coll Cardiol. 2010; 56(4):314. [PubMed: 20633824]
20. Jang IK, Bouma BE, Kang DH, Park SJ, Park SW, Seung KB, Choi KB, Shishkov M, Schlendorf K, Pomerantsev E, Houser SL, Aretz HT, Tearney GJ. Visualization of coronary atherosclerotic plaques in patients using optical coherence tomography: Comparison with intravascular ultrasound. J Am Coll Cardiol. 2002; 39(4):604–609. [PubMed: 11849858]
21. Sun Y, Park J, Stephens DN, Jo JA, Sun L, Cannata JM, Saroufeem RMG, Shung KK, Marcu L. Development of a dual-modal tissue diagnostic system combining time-resolved fluorescence spectroscopy and ultrasonic backscatter microscopy. Rev Sci Instrum. 2009; 80(6) art. no. 065104.
22. Sethuraman S, Aglyamov SR, Amirian JH, Smalling RW, Emelianov SY. Intravascular photoacoustic imaging using an IVUS imaging catheter. IEEE Trans Ultrason Ferroelectr Freq Control. 2007; 54(5):978–986. [PubMed: 17523562]
23. Sawada T, Shite J, Garcia-Garcia HM, Shinke T, Watanabe S, Otake H, Matsumoto D, Tanino Y, Ogasawara D, Kawamori H, Kato H, Miyoshi N, Yokoyama M, Serruys PW, Hirata K. Feasibility of combined use of intravascular ultrasound radiofrequency data analysis and optical coherence tomography for detecting thin-cap fibroatheroma. Eur Heart J. 2008; 29(9):1136–1146. [PubMed: 18397871]
24. Yang HC, Yin J, Hu C, Cannata J, Zhou Q, Zhang J, Chen Z, Shung KK. A dual-modality probe utilizing intravascular ultrasound and optical coherence tomography for intravascular imaging applications. IEEE Trans Ultrason Ferroelectr Freq Control. 2010; 57(12):2839–2843. [PubMed: 21156380]
25. Li X, Yin J, Hu C, Zhou Q, Shung KK, Chen Z. High-resolution coregistered intravascular imaging with integrated ultrasound and optical coherence tomography probe. Appl Phys Lett. 2010; 97(13) art. no. 133702.
26. Hsieh BY, Chen SL, Ling T, Guo LJ, Li PC. Integrated intravascular ultrasound and photoacoustic imaging scan head. Opt Lett. 2010; 35(17):2892–2894. [PubMed: 20808360]
27. Wei W, Li X, Zhou Q, Shung KK. Integrated ultrasound and photoacoustic probe for co-registered intravascular imaging. J Biomed Opt. 2011; 16(10) art. no. 106001.
28. Yang Y, Li X, Wang T, Kumavor PD, Aguirre A, Shung KK, Zhou Q, Sanders M, Brewer M, Zhou Q. Integrated optical coherence tomography, ultrasound and photoacoustic imaging for ovarian tissue characterization. Biomed Opt Express. 2011; 2(9):2551–2561. [PubMed: 21991547]
29. Xu X, Yen JT, Shung KK. A low-cost bipolar pulse generator for high frequency ultrasound applications. IEEE Trans Ultrason Ferroelectr Freq Control. 2007; 54(2):443–447. [PubMed: 17328342]
30. Sun L, Xu X, Richard WD, Feng C, Johnson JA, Shung KK. A high-frame rate duplex ultrasound biomicroscopy for small animal imaging in vivo. IEEE Trans Biomed Eng. 2008; 55(8):2039–2049. [PubMed: 18632366]

31. Sun L, Lien C, Xu X, Shung KK. In vivo cardiac imaging of adult zebrafish using high frequency ultrasound (45–75 MHz). Ultrasound Med Biol. 2008; 34(1):31–39. [PubMed: 17825980]

32. Zhou Q, Xu X, Gottlieb EJ, Sun L, Cannata JM, Ameri H, Humayun MS, Han P, Shung KK. PMN-PT single crystal, high-frequency ultrasonic needle transducers for pulsed-wave Doppler application. IEEE Trans Ultrason Ferroelectr Freq Control. 2007; 54(3):668–675. [PubMed: 17375836]

33. Madsen EL, Frank GR, McCormick MM, Deaner ME, Stiles TA. Anechoic sphere phantoms for estimating 3-D resolution of very-high-frequency ultrasound scanners. IEEE Trans Ultrason Ferroelectr Freq Control. 2010; 57(10):2284–2292. [PubMed: 20889416]

Biographies

Weibao Qiu was born in Jilin Province, China, in 1982. He received his B.S. degree from the Hefei University of Technology, Hefei, China, in 2004, and his M.S. degree from the State Key Laboratory of Precision Measurement Technology and Instruments, Tianjin University, Tianjin, China, in 2007. He worked at the RFID Research Center, ZTE Corporation, China, as a hardware/FPGA research engineer for two years after receiving his master's degree. He is currently a Ph.D. candidate in the Interdisciplinary Division of Biomedical Engineering, The Hong Kong Polytechnic University, Hong Kong, China. His research interests include digital signal processing, FPGA algorithms, high-speed circuit design, high-frequency ultrasound imaging systems, digital beamformers, coded excitation imaging, IVUS imaging, and Doppler imaging.

Yan Chen was born in Hebei Province, China. She obtained B.E. and M.Phil. degrees in 2006 and 2009, respectively, both from the Jingdezhen Ceramic Institute, Jingdezhen, China. She is now a Ph.D. candidate in the Department of Applied Physics, Hong Kong Polytechnic University, Hong Kong, China. Her research interests are piezoelectric materials and ultrasound transducers.

Xiang Li received a B.E. degree from Zhejiang University, China, in 2007 and M.S. and Ph.D. degrees from the University of Southern California (USC), Los Angeles, CA, in 2010 and 2012, respectively. He started his Ph.D. study in 2008 under the support of the USC Provost's Fellowship. In 2010, he won the Student Paper Competition Award at the IEEE International Ultrasonics Symposium, San Diego, CA. Under the direction of Dr. Qifa Zhou and Dr. K. Kirk Shung, Xiang is conducting his research in the NIH Ultrasonic Transducer Resource Center (UTRC) on high-frequency ultrasonic transducer technology, integrated IVUS-OCT imaging, and intravascular photoacoustic imaging.

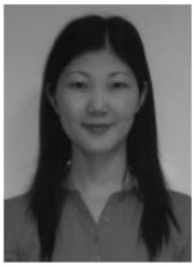

Yanyan Yu was born in Jilin Province, China. She received her B.S. and M.S. degrees from the Hefei University of Technology, Hefei, China, in 2006 and 2009, respectively. She worked at the Hefei Meiya Optoelectronic Technology Inc., China, as an image processing software engineer for nearly a year after receiving her master's degree. She is currently working as a research assistant in the Interdisciplinary Division of Biomedical Engineering, The Hong Kong Polytechnic University, Hong Kong, China. Her research interests include digital image processing, ultrasonic imaging, and the theory and applications of acoustic radiation force.

Wang Fai Cheng received his B.S. and M.Phil. degrees from the Hong Kong Polytechnic University, Hong Kong, China, in 2005 and 2008, respectively. Currently, he is a research assistant in the Department of Applied Physics, Hong Kong Polytechnic University, Hong Kong, China. His research interests include spintronics, ultrasound imaging, and narrow linewidth tunable lasers.

Fu Keung Tsang was born in Dongguan, China, in 1987. He received the B.S. degree in biomedical engineering in 2010 from the Hong Kong Polytechnic University, Kowloon, Hong Kong. He is currently a research assistant in the Interdisciplinary Division of Biomedical Engineering, The Hong Kong Polytechnic University, Hong Kong, China. His research interests include ultrasound coded excitation imaging and small animal imaging.

Qifa Zhou received his Ph.D. degree from the Department of Electronic Materials and Engineering at Xi'an Jiaotong University, China, in 1993. He is currently a Research Professor at the NIH Resource on Medical Ultrasonic Transducer Technology and the Department of Biomedical Engineering at the University of Southern California (USC), Los Angeles, CA. Before joining USC in 2002, he worked in the Department of Physics at Zhongshan University of China, the Department of Applied Physics at Hong Kong Polytechnic University, and the Materials Research Laboratory at The Pennsylvania State University.

Dr. Zhou is a senior member of IEEE (UFFC Society) and a member of the UFFC Society's Ferroelectric Committee. He is also a member of the Technical Program Committee of the IEEE International Ultrasonics Symposium. He is an Associate Editor of the *IEEE Transactions on Ultrasonics, Ferroelectrics, and Frequency Control*. His current research interests include the development of ferroelectric thin films, MEMS technology, nano-composites, modeling and fabrication of high-frequency ultrasound transducers and arrays for medical imaging applications, and photoacoustic imaging. He has published more than 100 papers in this area.

K. Kirk Shung obtained a B.S. degree in electrical engineering from Cheng-Kung University in Taiwan in 1968; an M.S. degree in electrical engineering from the University of Missouri, Columbia, MO, in 1970; and a Ph.D. degree in electrical engineering from the University of Washington, Seattle, WA, in 1975. He taught at The Pennsylvania State University, University Park, PA, for 23 years before moving to the Department of Biomedical Engineering, University of Southern California, Los Angeles, CA, as a professor in 2002. He has been the director of the NIH Resource on Medical Ultrasonic Transducer Technology since 1997.

Dr. Shung is a Life Fellow of IEEE and a fellow of the Acoustical Society of America and the American Institute of Ultrasound in Medicine. He is a founding fellow of the American Institute of Medical and Biological Engineering. He received the IEEE Engineering in Medicine and Biology Society Early Career Award in 1985 and was the coauthor of a paper that received the best paper award for the *IEEE Transactions on Ultrasonics, Ferroelectrics, and Frequency Control* (UFFC) in 2000. He was elected an outstanding alumnus of Cheng-Kung University in Taiwan in 2001. He was selected as the distinguished lecturer for the IEEE UFFC society for 2002–2003. He received the Holmes Pioneer Award in Basic Science from the American Institute of Ultrasound in Medicine in 2010. He was selected to receive the academic career achievement award from the IEEE Engineering in Medicine and Biology Society in 2011.

Dr. Shung has published more than 400 papers and book chapters. He is the author of the textbook *Principles of Medical Imaging*, published by Academic Press in 1992, and the textbook *Diagnostic Ultrasound: Imaging and Blood Flow Measurements*, published by CRC Press in 2005. He co-edited the book *Ultrasonic Scattering by Biological Tissues*, published by CRC Press in 1993. Dr. Shung's research interest is in ultrasonic transducers, high-frequency ultrasonic imaging, ultrasound microbeams, and ultrasonic scattering in tissues.

Jiyan Dai received his B.Sc. degree in physics from Fudan University in 1988, his M.S. degree in electrical engineering from Tsinghua University in 1991, and his Ph.D. degree in materials physics from the Chinese Academy of Sciences in 1994. He has worked at Northwestern University as a Research Associate for three years, and after one year working in the Institute of Materials Research and Engineering, Singapore, he joined Chartered Semiconductor Manufacturing Ltd. in Singapore in failure analysis. His research interests are materials science and medical ultrasound transducers. He joined the Department of Applied Physics at the Polytechnic University in 2001 as a lecturer, and is currently an Associate Professor. He has been working on a few projects in fabricating endoscopic and high-frequency ultrasound transducers and imaging systems.

Lei Sun was born in Shenyang, China. He received his B.S. degree in electrical engineering from the University of Science and Technology of China, Hefei, China, in 1996; his M.S. degree in electrical engineering from the Chinese Academy of Sciences, Beijing, China, in 2000; and his Ph.D. degree in bioengineering from The Pennsylvania State University, University Park, PA, in 2004.

Currently, he is an Assistant Professor in the Interdisciplinary Division of Biomedical Engineering, Hong Kong Polytechnic University, Hong Kong, China. From 2004 to 2008, he was a Postdoctoral Fellow and a Research Associate at the National Institutes of Health (NIH) Resource Center for Medical Ultrasonic Transducer Technology, University of Southern California, Los Angeles, CA. His research interests include ultrasonic and Doppler imaging, high-frequency ultrasound, magnetic-resonance-guided high-intensity focused ultrasound (HIFU), small animal imaging, cardiac imaging, ultrasonic tissue characterization, biomedical instrumentation, and biomedical signal and image processing.

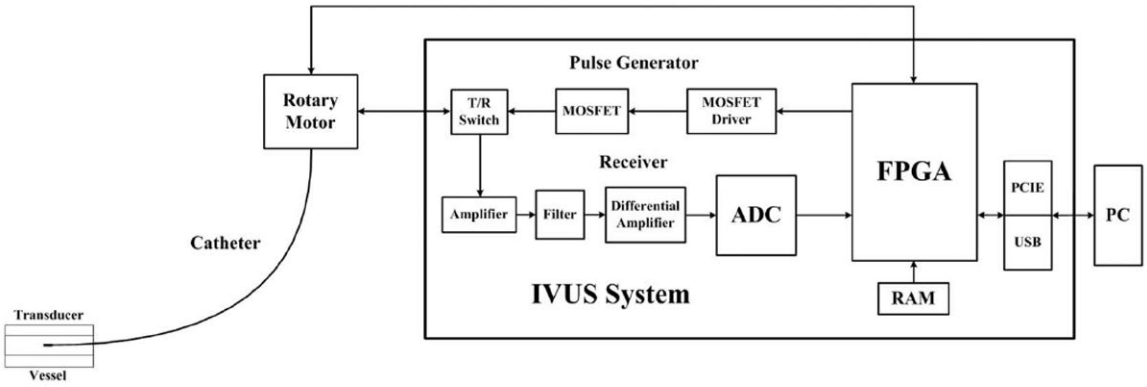

Fig. 1.
The block diagram of the open system for intravascular ultrasound (IVUS) imaging.

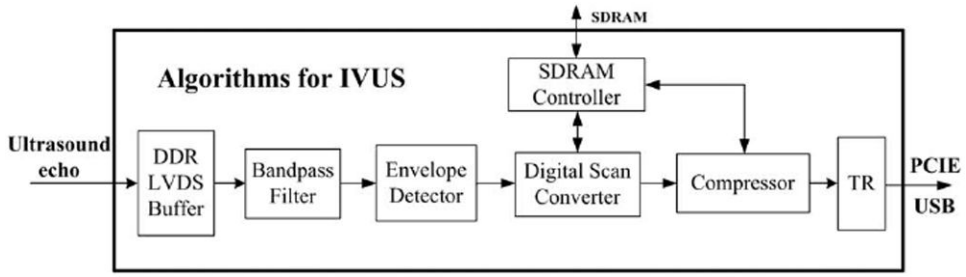

Fig. 2.
The algorithms implemented in the field-programmable gate array (FPGA) for real-time intravascular ultrasound (IVUS) imaging.

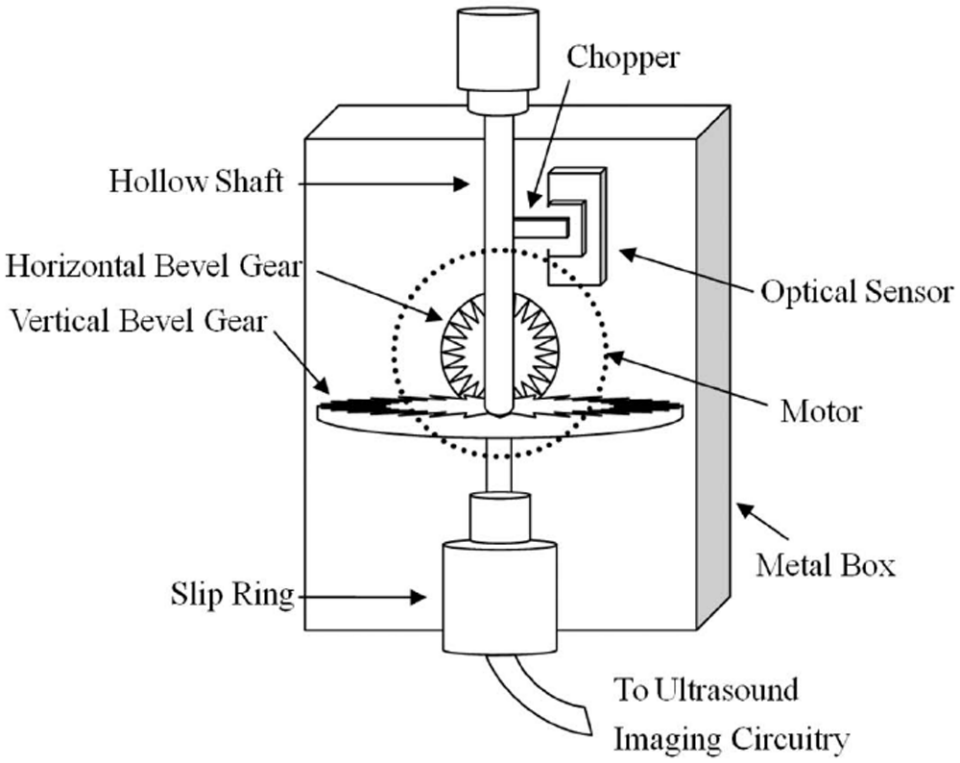

Fig. 3.
The detailed structure of the rotary motor.

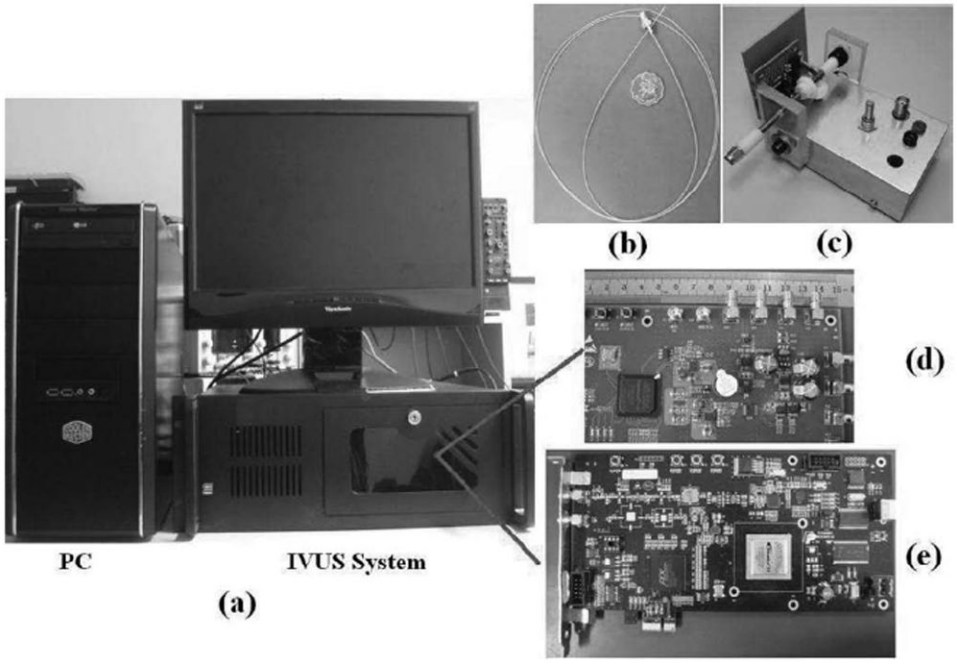

Fig. 4.
Photographs of (a) the entire open intravascular ultrasound (IVUS) system, (b) IVUS catheter, (c) small rotary motor, (d) highvoltage pulse generator, and (e) high-speed digital receiver.

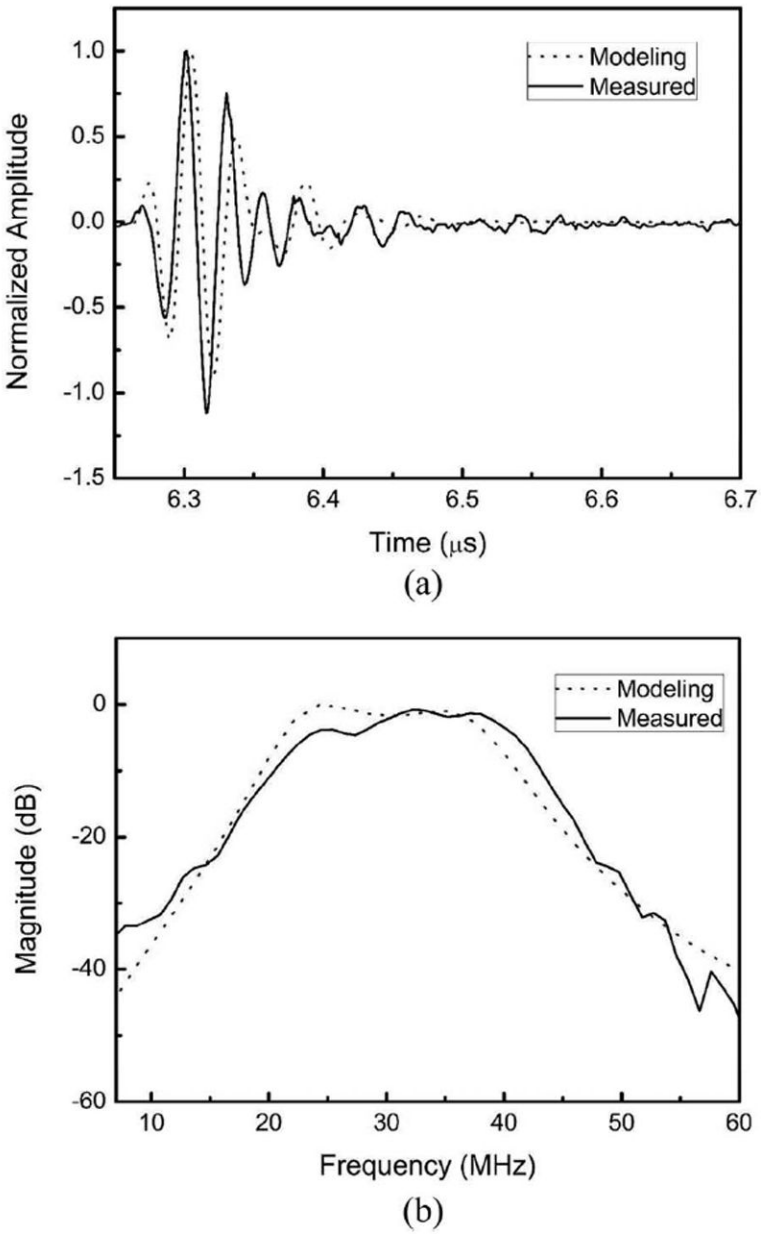

Fig. 5.

The (dash line) modeled and (solid line) measured (a) pulse-echo waveform and (b) frequency spectrum of the intravascular ultrasound (IVUS) catheter (measured results: 32 MHz center frequency, 62.7% bandwidth, and 25 dB insertion loss).

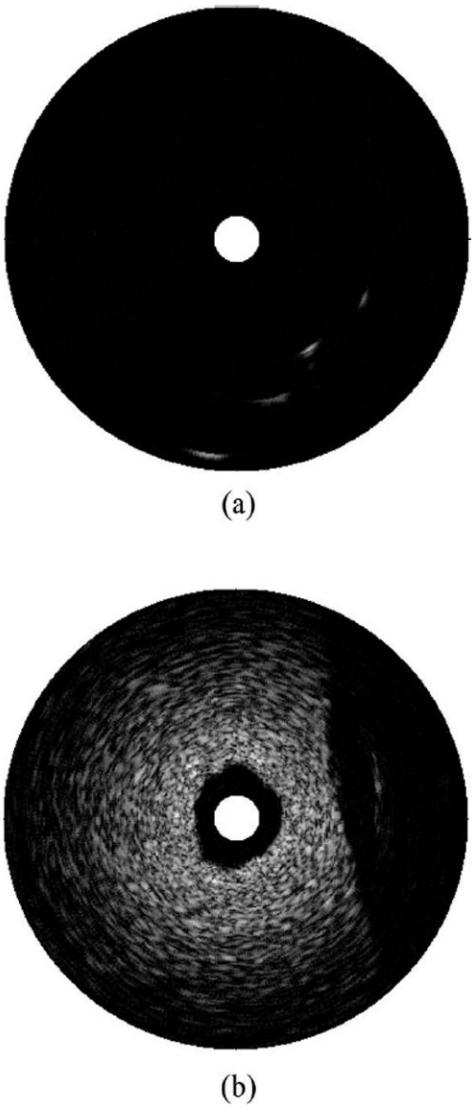

Fig. 6.
Phantom evaluation of the designed intravascular ultrasound (IVUS) system: (a) tungsten wire phantom image and (b) image of tissue-mimicking phantom.

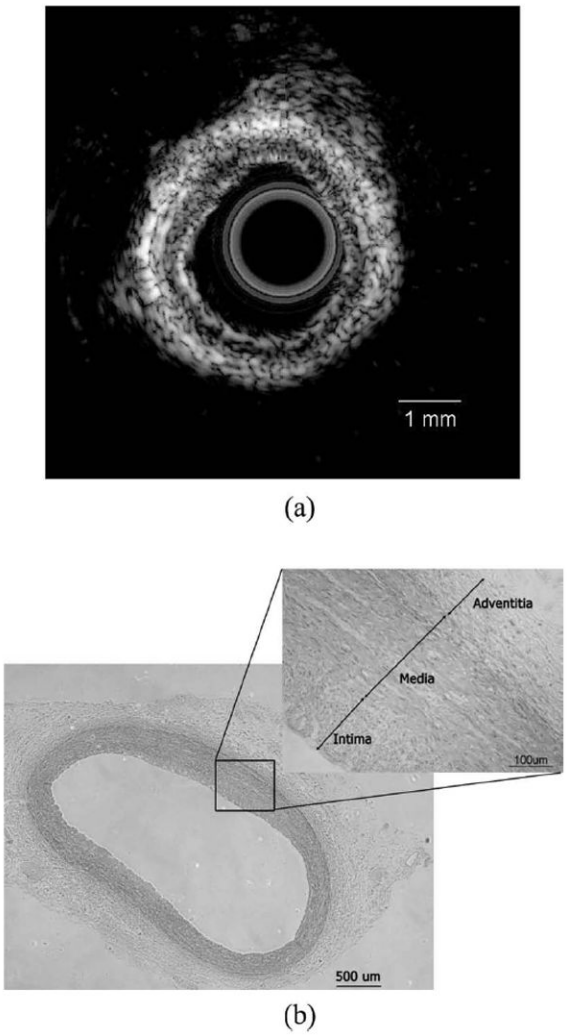

Fig. 7.
In vitro imaging of swine coronary artery by intravascular ultrasound (IVUS) and histology: (a) ultrasound image and (b) histological section.

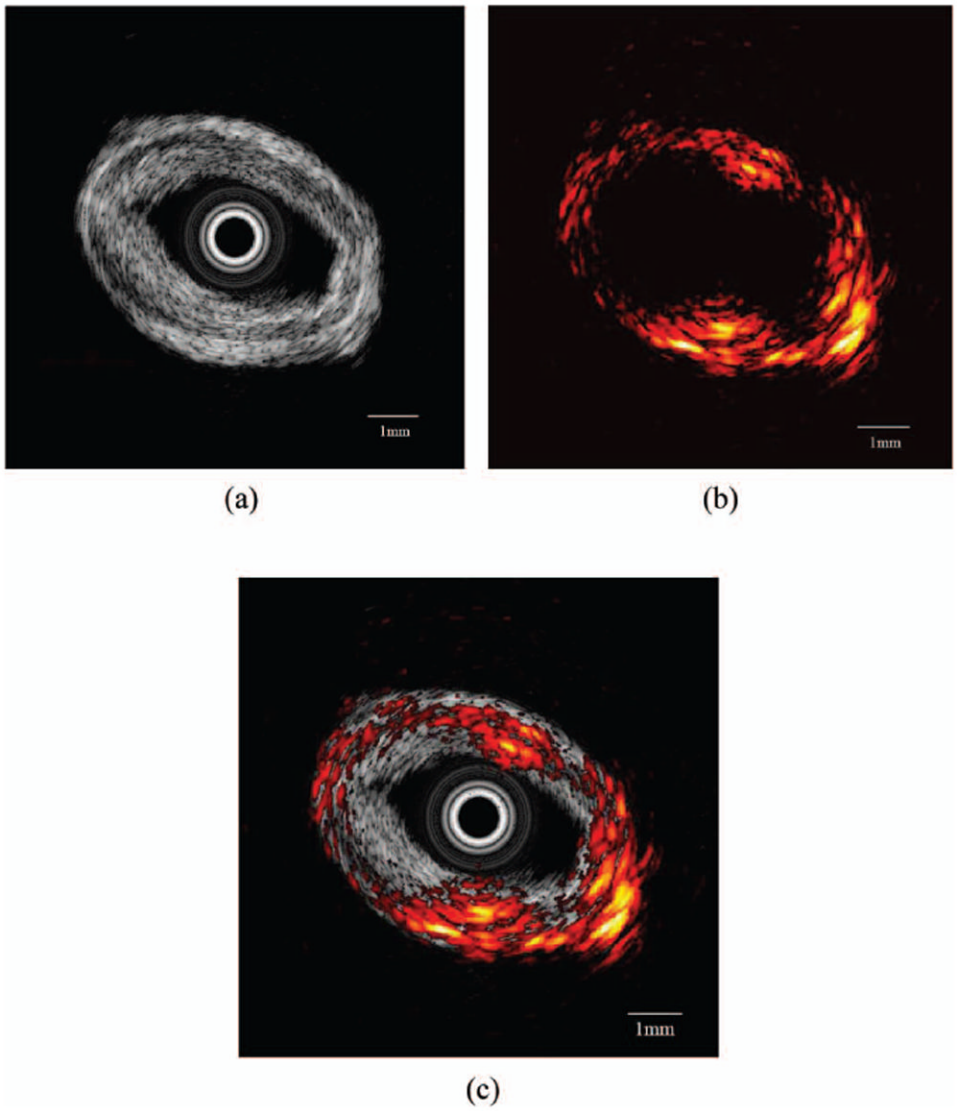

Fig. 8.
In vitro imaging of human coronary artery: (a) intravascular ultrasound (IVUS) image, (b) photoacoustic image, and (c) combined IVUS and photoacoustic image.

TABLE I

Electronics Performance of the Open System.

Article	Performance
Frequency range	20 to 80 MHz
High-voltage tunable pulse	Up to 160 V Vpp
Gain	47 dB
Gain fluctuation	±1.2 dB
Analog-to-digital converter (ADC)	11 bits, 200 MSPS
Minimum detectable signal	25 μV
Dynamic range	51 dB
Software improved dynamic range	55.8 dB
Data transferring speed	150 MB/s (PCIe)
	20 MB/s (USB)

TABLE II

Resource Utilization of the Field-Programmable Gate Array (FPGA).

Article	Resource utilization
Adaptive look-up tables (ALUTs)	4855 (10%)
Pins	216 (44%)
DSP block 9-bit elements	64 (22%)
Memory bits	53152 (2%)
PLLs	2 (33%)

DSP = digital signal processing; PLL = phase-locked loop.